# $J_2$-Modified GVE-Based MPC for Formation Flying Spacecraft

Louis Breger* and Jonathan P. How†

*MIT Department of Aeronautics and Astronautics*

**Formation flying is an enabling technology for many future space missions. This paper presents an MPC controller that uses dynamics based on a modified version of Gauss' Variational Equations which incorporates osculating $J_2$ effects. A linear parameter-varying version of existing dynamics is developed, creating a highly accurate model that can easily be embedded in the MPC controller design. The linearization assumptions are shown to be consistent with typical formation flying scenarios. The controller is demonstrated on an MMS-like formation flying mission in a highly elliptical orbit using a commercial orbit propagator with realistic disturbances (including $J_2$). These simulations show that formation flying using MPC with $J_2$-modified GVEs requires fuel expenditures comparable to using unmodified GVEs in simulations with no $J_2$ effects.**

## I. Introduction

In recent years, a variety of methods of controlling spacecraft formations have been proposed.[5,8,7,6,17,4] The model predictive control (MPC) approach is well-suited to formation control because it emphasizes planning rather than immediate feedback, directly accounts for realistic mission constraints, and explicitly optimizes fuel usage ($\|\Delta V\|_1$). The planning aspect of model predictive control is effective when system dynamics are well known, as is the case for space vehicles. Planning has a particular advantage over continuous control, in that it allows for the type of impulsive "bang-off-bang" control laws often found in optimal control and typically does not engage in constant thrusting, which is often inconsistent which science data collection. Constraints on spacecraft usually include restrictions on when and how much thruster firing can occur and how much state error can be tolerated; all three types of constraints are easily incorporated into an optimization-based planner. In any spacecraft, fuel is a limited resource. This limitation is compounded in a spacecraft formation, where fuel must be expended regularly to maintain the formation, which also means that running out of fuel in a single spacecraft ends the entire mission. An MPC schemes allows the fuel cost function to be made explicit in the optimization. Often in the literature, optimization-based control refers to large nonlinear problems that take hours or days to solve. However, the optimizations described in this paper are linear programs (LPs) that take fractions of a second to solve, which makes them well-suited for real-time implementation. Here, a model predictive control system for formation flying spacecraft is extended to use dynamics that explicitly account for the effects of $J_2$.

A detailed description of a linear, convex MPC approach to formation flying is found in Ref. 4. In that paper, Hill's and Lawden's equations of motion are used as the system dynamics for relative satellite motion. Hill's equations describe relative satellite motion in a circular orbit and are linear time-invariant (LTI). Lawden's equations describe relative satellite motion in an elliptic orbit of arbitrary eccentricity and are linear parameter-varying (LPV). Linear parameter-varying equations represent a compromise between LTI and nonlinear dynamics: they retain the ability to easily include the effect of inputs associated with linear dynamics, which greatly simplifies the control design, while still accurately capturing the dynamics for small discretization time steps. Both Hill's and Lawden's equations are linearized according to spacecraft separation and consequently degrade in accuracy for large formations represented in a single frame. More recently, linear parameter-varying dynamics known as Gauss' Variational Equations (GVEs) have been used

*Research Assistant, MIT Department of Aeronautics and Astronautics, lbreger@mit.edu

†Associate Professor, MIT Department of Aeronautics and Astronautics, (AIAA Associate Fellow) jhow@mit.edu

that propagate Keplerian orbital element representations of spacecraft state.[20] This approach combined with differential orbital element representations of desired spacecraft state and error allowed much larger formations to be controlled effectively in elliptical orbits of arbitrary eccentricity.

A limitation of the orbital element approach in Ref. 20 is that it does not account for the effects of the $J_2$ disturbance. That limitation severely impacted the controller's ability to produce realistic planned trajectories. In this paper, the relative orbital element approach to planning used in Ref. 20 has been extended to use the $J_2$-modified GVEs that are found in Ref. 18. The $J_2$-modified GVEs are used to form a set of linear parameter-varying dynamics that is then used in a model predictive control system. The result is a controller that retains the advantages of the GVE-based controller used in Ref. 20, but uses a more accurate dynamics model, thereby improving plan tracking and fuel efficiency. After developing the dynamics, this paper evaluates the validity of the linearizing assumptions used and then applies the new controller to a highly elliptic formation flying mission with widely separated satellites in the presence of realistic disturbances. Simulations show that controlling a formation in the presence of $J_2$ disturbances using MPC with $J_2$-modified GVEs requires fuel expenditures comparable to the approach using unmodified GVEs when $J_2$ disturbances are not simulated.

## II. $J_2$-Modified GVEs and Linearization Validity

Gauss' Variational Equations (GVEs) are derived in Ref. 11 and are reproduced here for reference

$$\frac{d}{dt}\begin{pmatrix} a \\ e \\ i \\ \Omega \\ \omega \\ M \end{pmatrix} = \begin{pmatrix} 0 \\ 0 \\ 0 \\ 0 \\ 0 \\ n \end{pmatrix} + \begin{pmatrix} \frac{2a^2 e \sin f}{h} & \frac{2a^2 p}{rh} & 0 \\ \frac{p \sin f}{h} & \frac{(p+r)\cos f + re}{h} & 0 \\ 0 & 0 & \frac{r\cos\theta}{h} \\ 0 & 0 & \frac{r\sin\theta}{h\sin i} \\ -\frac{p\cos f}{he} & \frac{(p+r)\sin f}{he} & -\frac{r\sin\theta\cos i}{h\sin i} \\ \frac{b(p\cos f - 2re)}{ahe} & -\frac{b(p+r)\sin f}{ahe} & 0 \end{pmatrix} \begin{pmatrix} \mathbf{u_r} \\ \mathbf{u}_\theta \\ \mathbf{u_h} \end{pmatrix} \tag{1}$$

where the state vector elements are $a$ (semimajor axis), $e$ (eccentricity), $i$ (inclination), $\Omega$ (right ascension of the ascending node), $\omega$ (argument of periapse), and $M$ (mean motion). The other terms in the variational expression are $p$ (semi-latus rectum), $b$ (semiminor axis), $h$ (angular momentum), $\theta$ (argument of latitude), $r$ (magnitude of radius vector), and $n$ (mean motion). All units are in radians, except for semimajor axis and radius (meters), angular momentum (kilogram $\cdot$ meters$^2$ per second), mean motion (1/seconds), and eccentricity (dimensionless). The input acceleration components $\mathbf{u_r}$, $\mathbf{u}_\theta$, and $\mathbf{u_h}$ are in the radial, in-track, and cross-track directions, respectively, of an LVLH frame centered on the satellite and have units of meters per second$^2$. The form of the GVEs can be more compactly expressed as

$$\dot{\mathbf{e}_0} = A(\mathbf{e}_0) + B(\mathbf{e}_0)\mathbf{u} = A(\mathbf{e}_0) + \frac{\partial \dot{\mathbf{e}}_0}{\partial \mathbf{u}}\mathbf{u} \tag{2}$$

where $\mathbf{e}_0$ is the osculating state vector in Eq. 1, $B(\mathbf{e}_0)$ is the input effect matrix, $\mathbf{u}$ is the vector of thrust inputs in the radial, in-track, and cross-track directions, and $A(\mathbf{e}_0) = (\ 0 \quad 0 \quad 0 \quad 0 \quad 0 \quad \sqrt{\mu/a^3}\ )^T$, where $\mu$ is the gravitational parameter.

Likewise, the equations of motion of the mean orbital element state vector $\mathbf{e}$ are given by

$$\dot{\mathbf{e}} = \bar{A}(\mathbf{e}) + \frac{\partial \dot{\mathbf{e}}}{\partial \mathbf{u}}\mathbf{u} \tag{3}$$

where $\bar{A}$ is explicitly a function of the mean state and implicitly a function of $J_2$ and can be found in Ref. 10. Although Equations 2 and 3 appear similar, it is their differences that are at the crux of this paper. Equation 2 describes the motion of a spacecraft's osculating orbit and is the form of the classical GVEs. Previous work[20] established that it is valid and effective to linearize the GVEs and use them for model predictive control. However, the GVEs incorporate neither the absolute nor the relative effects of $J_2$ on a satellite's orbit. Conversely, Eq. 3 describes the motion of an orbit in a set of mean orbital elements, where the secular effects of $J_2$ are incorporated and harmonics are removed. This form of the dynamics is useful for controlling the secular drift between satellites in a formation, but does not describe precise physical motion and has limited application to missions requiring precise control. Furthermore, the form is nonlinear in

terms of the relative state, which accurately captures system dynamics, but makes optimization of control inputs difficult. However, by utilizing the linearized propagation and rotation matrices developed in Ref. 18, a relative form of the equations of motion in Eq. 3 will be developed that incorporates the osculating effects of $J_2$, remains linear parameter varying, and is valid for large spacecraft separations and reference orbit eccentricities.

To find the control influence matrix of the mean orbital element equations of motion, the following identity is employed

$$\frac{\partial \dot{\mathbf{e}}}{\partial \mathbf{u}} = \frac{\partial \dot{\mathbf{e}}}{\partial \dot{\mathbf{e}}_0} \times \frac{\partial \dot{\mathbf{e}}_0}{\partial \mathbf{u}} \tag{4}$$

The relation between the mean orbital element state vector and the osculating orbital element state vector is given by the function $f$

$$\mathbf{e} = f(\mathbf{e}_0) \tag{5}$$

which can be found in the appendix of Ref. 9. Thus,

$$\dot{\mathbf{e}} = \frac{\partial f}{\partial \mathbf{e}_0}\dot{\mathbf{e}}_0 \quad \Rightarrow \quad \frac{\partial \dot{\mathbf{e}}}{\partial \dot{\mathbf{e}}_0} = \frac{\partial f}{\partial \mathbf{e}_0} \tag{6}$$

Substituting Eq. 6 and the $B$ matrix from Eq. 1 into Eq. 4 gives

$$\frac{\partial \dot{\mathbf{e}}}{\partial \mathbf{u}} = \frac{\partial f(\mathbf{e}_0)}{\partial \mathbf{e}_0} B(\mathbf{e}_0) \tag{7}$$

which yields the equations of motion of the mean orbit in terms of the osculating orbital state vector $\mathbf{e}_0$ (the mean elements may be considered a function of the osculating elements) and an input vector $\mathbf{u}$ as

$$\dot{\mathbf{e}} = \bar{A}(\mathbf{e}) + \frac{\partial f}{\partial \mathbf{e}_0} B(\mathbf{e}_0)\mathbf{u} \tag{8}$$

The actual mean orbit $\mathbf{e}$ is now defined in terms of a desired mean orbit $\mathbf{e}_d$ and a vector offset $\zeta$

$$\mathbf{e} = \mathbf{e}_d + \zeta \tag{9}$$

Rearranging this expression and applying Eq. 3 gives

$$\dot{\mathbf{e}} - \dot{\mathbf{e}}_d = \dot{\zeta} = \bar{A}(\mathbf{e}) - \bar{A}(\mathbf{e}_d) + \frac{\partial \dot{\mathbf{e}}}{\partial \mathbf{u}}\mathbf{u} - \frac{\partial \dot{\mathbf{e}_\mathbf{d}}}{\partial \mathbf{u}}\mathbf{u} \tag{10}$$

Since inputs can only be applied at the actual location of the orbit, the term $\frac{\partial \dot{\mathbf{e}_\mathbf{d}}}{\partial \mathbf{u}}\mathbf{u}$ is dropped, yielding the expression

$$\dot{\zeta} = \bar{A}(\mathbf{e}) - \bar{A}(\mathbf{e}_d) + \frac{\partial \dot{\mathbf{e}}}{\partial \mathbf{u}}\mathbf{u} \tag{11}$$

The linearization approximation

$$\bar{A}(\mathbf{e}) - \bar{A}(\mathbf{e}_d) \approx \left.\frac{\partial \bar{A}}{\partial \mathbf{e}}\right|_{\mathbf{e}_d} \zeta \equiv \bar{A}^*(\mathbf{e}_d)\zeta \tag{12}$$

is then used to find the equations of motion of the mean element offset $\zeta$

$$\dot{\zeta} = \bar{A}^*(\mathbf{e}_d)\zeta + \frac{\partial \dot{\mathbf{e}}}{\partial \mathbf{u}}\mathbf{u} \tag{13}$$

where the terms of the matrix function $\bar{A}^*$ are given in Ref. 10. Equation 13 provides a linear description of the relative motion of relative mean orbital elements. However, to maximize the ability of the planner to exploit natural dynamics and operate with tight performance constraints, the dynamics will be further developed to operate on an osculating state vector.

The formation will now be specified in terms of the osculating orbit $\mathbf{e}_0$, an osculating desired orbit $\mathbf{e}_{0d}$, and an osculating orbital offset $\zeta_0$ between them,

$$\mathbf{e}_0 = \mathbf{e}_{0d} + \zeta_0 \tag{14}$$

Defining the mean elements in terms of the osculating elements gives $\mathbf{e} = f(\mathbf{e}_0)$ and $\mathbf{e}_d = f(\mathbf{e}_{0d})$, which can be used to form a relative state and linearized rotation matrix

$$\zeta = f(\mathbf{e}_0) - f(\mathbf{e}_{0d}) \approx \left.\frac{\partial f}{\partial \mathbf{e}_0}\right|_{\mathbf{e}_{0d}} \zeta_0 \tag{15}$$

Defining the matrix function $D$ (available in Ref. 18),

$$D(\mathbf{e}_{0d}) \equiv \left.\frac{\partial f}{\partial \mathbf{e}_0}\right|_{\mathbf{e}_{0d}} \tag{16}$$

and substituting into Eq. 7 and then into Eq. 13 yields

$$\dot{\zeta} = \bar{A}^*(f(\mathbf{e}_{0d}))\zeta + D(\mathbf{e}_0)B(\mathbf{e}_0)\mathbf{u} \tag{17}$$

This form of the relative equations of motion is nonlinear in terms of the osculating absolute state $\mathbf{e}_0$. Making the linearizing assumption

$$D(\mathbf{e}_0)B(\mathbf{e}_0) = D(\mathbf{e}_{0d} + \zeta_0)B(\mathbf{e}_{0d} + \zeta_0) \tag{18}$$

$$\approx D(\mathbf{e}_{0d})B(\mathbf{e}_{0d}) \tag{19}$$

allows the relative equations of motion to be rewritten as

$$\dot{\zeta} = \bar{A}^*(f(\mathbf{e}_{0d}))\zeta + D(\mathbf{e}_{0d})B(\mathbf{e}_{0d})\mathbf{u} \tag{20}$$

which has a desired osculating orbit $\mathbf{e}_{0d}$ and is linear in terms of the relative mean state $\zeta$. The equations of motion in Eq. 20 are still not suited to control of the osculating relative orbit in the presence of $J_2$, because they describe the derivative of the mean state. The useful form (from a planning perspective) that is linear in the relative osculating state and describes the evolution of that state will be derived in the following subsection where the dynamics are discretized.

### A. Extension to Discrete Time

To use Eq. 20 in an optimization-based controller of the type used in Ref. 20, it must first be discretized. Reference 18 introduces the state transition matrix $\bar{\Phi}$, which is the discrete form of the continuous matrix $\bar{A}^*(f(\mathbf{e}_{0d}))$, and is defined such that

$$\zeta(t_1) = \bar{\Phi}^*(\mathbf{e}_d, t_1, t_0)\zeta(t_0) \tag{21}$$

where $t_0$ is the time of the initial state and $t_1$ is the time of the final state. The analytic definition of the matrix $\bar{\Phi}^*$ (an implicit function of $J_2$ and a highly nonlinear function of the mean absolute elements) is included in appendices of Ref. 18.

These dynamics can now be formulated exclusively in terms of the osculating state. Using Eq. 15, define $D^{-1}$ as

$$D^{-1} \equiv \left.\frac{\partial \mathbf{e}_0}{\partial f}\right|_{\mathbf{e}_{0d}} \tag{22}$$

Substituting Eqs. 16 and 22 into Eq. 21 yields

$$\zeta_0(t_1) \approx D^{-1}(\mathbf{e}_{0d}(t_1))\bar{\Phi}^*(\mathbf{e}_d, t_1, t_0)D(\mathbf{e}_{0d}(t_0))\zeta_0(t_0)$$

The analogous discrete form of the control influence matrix $B$ on the osculating state is then given by

$$\Gamma(e_{0d}, t, t_0) = \int_{t_0}^{t} D^{-1}(\mathbf{e}_{0d}(t))\bar{\Phi}^*(\mathbf{e}_d, t, \tau)D(\mathbf{e}_{0d}(\tau))B(e_{0d}(\tau))d\tau \tag{23}$$

which uses a zero-order hold assumption for the inputs. Thus, combining Eqs. 21 and 23 yields the discrete time equations of motion

$$\zeta_0(t_1) \approx D^{-1}(\mathbf{e}_{0d}(t_1))\bar{\Phi}^*(\mathbf{e}_d, t_1, t_0)D(\mathbf{e}_{0d}(t_0))\zeta_0(t_0) + \Gamma(\mathbf{e}_{0d}, t_1, t_0)\mathbf{u} \tag{24}$$

which are the linear parameter-varying discrete equations of motion for a relative osculating orbit in the presence of $J_2$.

### B. Validity of Linear Approximation

Reference 20 showed that the approximation $B(\mathbf{e}_{0d}) \approx B(\mathbf{e}_{0d} + \zeta)$, which is used to derive Eq. 24, is a sufficiently close approximation for levels of state error, $\zeta_0$, that would normally be expected in spacecraft formation flying missions. In order to use Eq. 24 for linear control, it must also be shown that the linearized rotation and transition combination $D^{-1}(\mathbf{e}_{0d}(t_1))\bar{\Phi}^*(f(\mathbf{e}_{0d}(t_0)), t_1, t_0)D(\mathbf{e}_{0d}(t_0))$ remains a close approximation for expected values of $\zeta_0$. This matrix has been shown to have low linearization error for a wide range of reference orbit eccentricities and spacecraft errors[18] in excess of 10 kilometers, which is larger than the state error that would be tolerated in most spacecraft formation flying missions.

### C. Calculating the $\Gamma$ matrix

The discrete control effect matrix is defined as a matrix integral in Eq. 23. One way to calculate this matrix is by computing its derivative and numerically integrating. However, in practice this is a computationally intensive approach that may not be consistent with real-time controller implementation. An alternate approach computes $\Gamma$ using the matrix exponential of the continuous matrix $A^*$

$$\Gamma(\mathbf{e}_{0d}, t_1, t_0) \approx e^{A^*(t_1 - t_0)} B(\mathbf{e}_{0d}(t_0)) \tag{25}$$

This approach assumes that the effects of $J_2$ on the control influence matrix are negligible and that very little change occurs in the $A^*$ matrix over the period of a time step. An analogous assumption is made for the continuous $B$ matrix in Ref. 10. For small time steps (relative to the period of the orbit) this approach produces nearly identical $\Gamma$ matrices in a small fraction of the time required to solve for $\Gamma$ numerically (typically more than 100 times faster). Figure 1 shows how the evaluation of $\Gamma$ using Eq. 25 degrades as the discretization time step is increased for a highly eccentric, MMS-like orbit ($e \approx 0.8$). In the figure, $\Delta\Gamma$ refers to the difference between the $\Gamma$'s calculated using Eq. 25 and Eq. 25, respectively. For each time step, a series of $\Delta\Gamma$ matrices are evaluated and the matrix with the largest induced 2-norm is used to represent the discretization error. The figure indicates that the 86 second time step used is associated with just over 2% error between the $\Gamma$ matrices. If this error is too large, the time step can be made smaller or the numerical integration method can be used.

Another method of calculating the $\Gamma$ matrix uses a small time-step approximation by assuming that inputs can be applied through a double integrator model of the dynamics in an LVLH frame. The resulting LVLH state perturbations can then be rotated into relative orbital elements using the following linearized rotation matrix

$$\zeta = M(\mathbf{e}_{0d})\mathbf{x} \tag{26}$$

where $\mathbf{x} = [\ x \quad y \quad z \quad \dot{x} \quad \dot{y} \quad \dot{z}\ ]$ is a state vector in the LVLH frame centered on the absolute orbit $\mathbf{e}_{0d}$. The components of $\mathbf{x}$ are the radial, in-track, and cross-track position and velocity components in the LVLH frame, respectively. The elements of the $6 \times 6$ rotation matrix $M(\mathbf{e}_{0d})$ are known analytically and can be found in Appendix G of Ref. 10.

The continuous input matrix $\mathbf{B}_c$ for acceleration inputs is $\mathbf{B}_c = [0_3 \quad I_3]^T$, which when discretized with a time step $t_1 - t_0$ using the double integrator system has the discrete form[3]

$$\mathbf{B}_d = \begin{bmatrix} \frac{1}{2}(t_1 - t_0)^2 I_3 \\ (t_1 - t_0) I_3 \end{bmatrix} \tag{27}$$

where $0_3$ is a $3 \times 3$ matrix of zeros and $I_3$ is a $3 \times 3$ identity matrix. The product $\mathbf{B}_d\mathbf{u}$ yields a state perturbation in the LVLH frame, which can be rotated back into differential orbital elements using the $M$ matrix to become a differential element perturbation as a result of the input. Thus,

$$\Gamma(\mathbf{e}_{0d}, t_1, t_0) \approx M(\mathbf{e}_{0d}) \begin{bmatrix} \frac{1}{2}(t_1 - t_0)^2 I_3 \\ (t_1 - t_0) I_3 \end{bmatrix} \tag{28}$$

This approach has the dual advantages of accounting for $J_2$ in the formulation of the $M$ matrix and of allowing the analytic calculation of $\Gamma$.

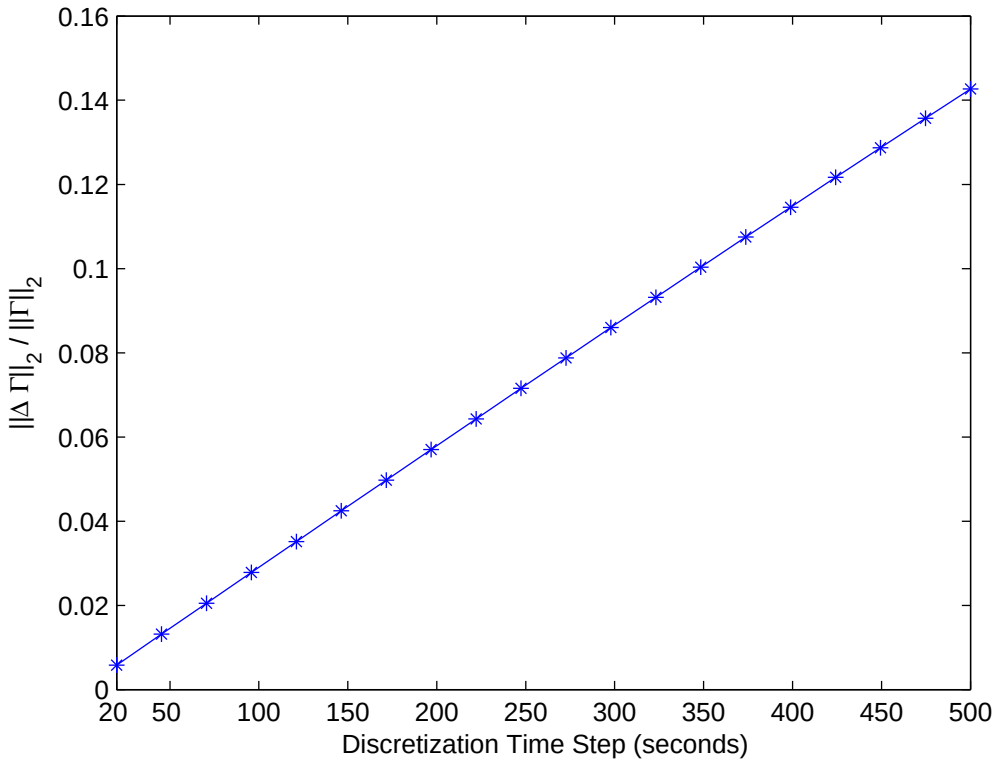


**Fig. 1**: Difference between integrated and approximated $\Gamma$ for different discretization times.

## III. Model Predictive Control Using $J_2$-Modified GVEs

Reference 4 showed that given a valid set of linearized dynamics and a desired trajectory, a model predictive controller can be designed for a spacecraft formation that allows for arbitrarily many convex terminal and intermediate state conditions, as well as sensor noise robustness requirements. This controller is implemented on each spacecraft using a linear programming formulation. The general form of the optimization performed by the controller is

$$\min \|\mathbf{u}\|_1 \quad \text{subject to} \quad \mathbf{A}_{\text{cons}}\mathbf{u} \leq \mathbf{b}_{\text{cons}} \tag{29}$$

where $\mathbf{u}$ is a vector of potential control inputs and the matrix $\mathbf{A}_{\text{cons}}$ and the vector $\mathbf{b}_{\text{cons}}$ are formed based on the input dynamics and problem constraints. Note that the one-norm captures the $\Delta V$ fuel cost.

The discrete dynamics in Eq. 20 are used to incorporate the linearized $J_2$-modified GVE-based equations of motion in the MPC formulation. Solutions to the optimization posed in Eq. 29 usually take the form of classical "bang-off-bang" optimal control laws. Figure 2 shows a typical plan to correct a small orbital element error. Note that although only two elements begin with errors, the optimized solution requires some elements to deviate from their desired states in order to minimize overall fuel use. Furthermore, unlike plans generated using the linearized relative GVEs in Ref. 20, the plan generates a trajectory that includes curved paths. These coasting regions make use of the natural motions induced by $J_2$ to correct state error, rather than using control to eliminate the effects of $J_2$ or using the mean elements as a filter to ignore those effects.

Solving the optimization in Eq. 29 with 1000 discretization steps and a terminal constraint has required less than 0.05 seconds on a 3 GHz computer for all simulations done. Formulating the matrices used in the optimization always takes less than 10 seconds, far less than the 86 second discretization time step. The time required to formulate the problem will increase as the discretization step is made smaller and additional constraints are added. A more complicated formulation could still be implemented in a real-time system by specifying that thrusting not begin for several time steps into the plan. This will result in a plan that does not require action until some specified time in the future when it is certain that the formulation and optimization will have been completed.

In Section V, spacecraft are controlled to reference trajectories. However, an alternate formation maintenance approach would be to use error boxes. In Ref. 4, position error boxes are demonstrated, but

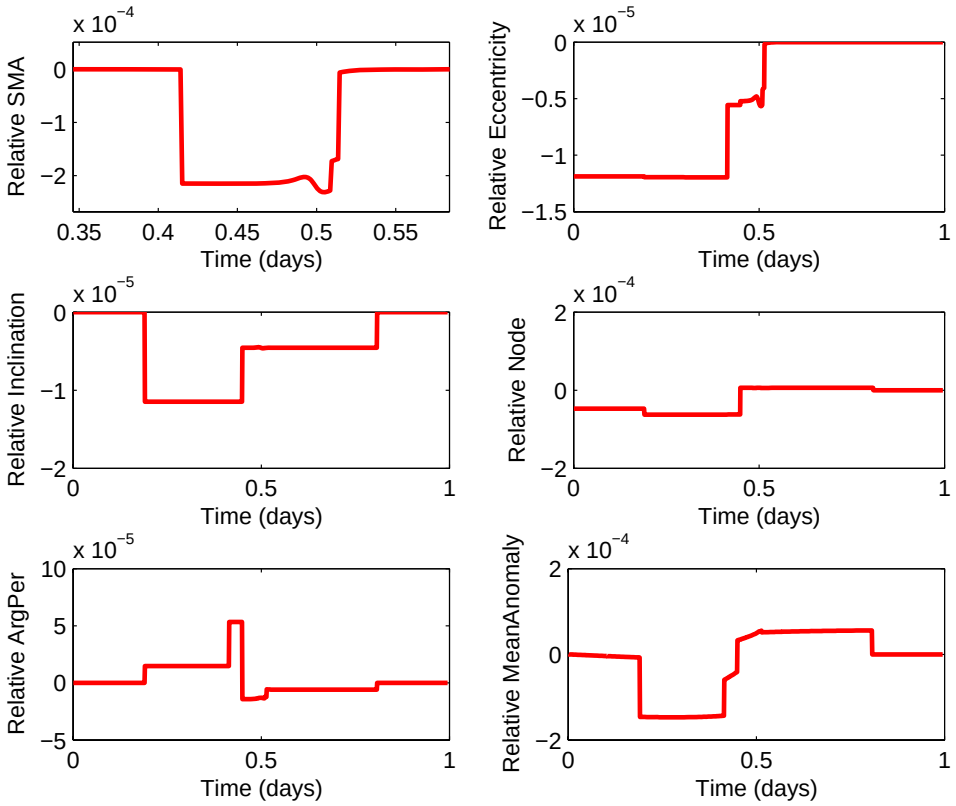


**Fig. 2:** Example of a plan generated using MPC with $J_2$-modified GVEs (lines indicate relative state error)

formulations for semimajor axis error boxes and velocity error boxes are also presented. Position is a convenient bounding mechanism for a formation flying mission, because it coincides well with science requirements on the accuracy of the formation geometry shape. When the formation geometry is specified in orbital elements, it is most convenient to use a six dimensional error box with bounds on each of the state elements. This approach, while simple and convenient for enforcing acceptable relative drift levels, does not map well into the position error box constraints typical of previous performance specifications. To transition between LVLH states, $\mathbf{x}$, and relative orbital element states, $\zeta_0$, the rotation matrix $M(\mathbf{e}_{0_d})$ from Eq. 26 is used, where

$$\zeta_0 = M(\mathbf{e}_{0_d})\mathbf{x} \tag{30}$$

It is possible to enforce relative position and relative velocity error box constraints using the $M(\mathbf{e})$ matrix by formulating the optimization problem in Eq. 29 with constraints at any step $k$ where it is desired that the spacecraft remain inside an error box about the full state.

$$\mathbf{x}_{\min} \leq M^{-1}(\mathbf{e}_{0_d})\zeta_0 \leq \mathbf{x}_{\max} \tag{31}$$

where $\mathbf{x}_{\max}$ is one corner of the error box and $\mathbf{x}_{\min}$ is the opposing corner. Here, $\mathbf{e}_{0_d}$ is the desired state and $\zeta_0$ is the state error. To exclusively enforce a partial state error box (*e.g.,* a position box), an additional matrix $H$ can be premultiplied by $M(\mathbf{e}_0)$ in both constraints to only retain the desired components. Note that formations in highly eccentric orbits will naturally change geometry dramatically over the course of an orbit and it may only be desirable to enforce error boxes at particular true anomalies (*e.g.,* apogee).

## IV. General Drift-free Tetrahedron Initial Conditions

The MMS mission will require spacecraft to form very large tetrahedron shapes, while simultaneously not drifting with respect to one another. Drift-free designs based on Hill's and Lawden's equations are valid only

for formations with short baselines, because of the linearization assumptions inherent in the specification of the frames in the derivation of the dynamics. For any group of spacecraft, a no-drift requirement is equivalent to requiring that all spacecraft have the same orbital energy, which is also equivalent to stating that all spacecraft have the same semimajor axis. For a formation specified in differential orbital elements, this is the same as requiring that the desired differential semimajor axes for all spacecraft in the formation be zero. Thus, in differential orbital elements it is trivial to design a drift-free formation, however, the curvilinear nature of the elements makes describing and manipulating general tetrahedron shapes complicated.

One approach is to begin with tetrahedron coordinates in a rectilinear frame (such as LVLH or ECEF) and then convert those coordinates into orbital element perturbations. However, producing the desired orbital element differences for a tetrahedron requires knowledge of the full relative state in a rectilinear frame, including both position and velocity. If the only constraint on the formation geometry is that the satellite positions form a tetrahedron shape, then the velocity must be selected based on additional criteria.

A regular tetrahedron with sides of length $s$ can be described in a rectilinear frame using the coordinates (given in $x$, $y$, $z$ triples)

$$\text{Sat}_1 = (0, 0, \frac{\sqrt{3}}{3}s) \qquad \text{Sat}_2 = (0, \frac{1}{2}s, -\frac{\sqrt{3}}{6}s) \qquad \text{Sat}_3 = (0, -\frac{1}{2}s, -\frac{\sqrt{3}}{6}s) \qquad \text{Sat}_4 = (\frac{\sqrt{6}}{3}s, 0, 0)$$

Using $M$ matrix from Eq. 26, these projections from LVLH coordinates to differential orbital elements can be used to establish three and six dimensional "box" constraints on spacecraft position and velocity of the type discussed in Refs. 4 and 19.

The desired LVLH state of satellite $i$ can be expressed as the concatenation of a position vector $\mathbf{p}_i$ and a velocity vector $\mathbf{v}_i$, each with states in the $x$, $y$, and $z$ directions.

$$\mathbf{x}_i = \begin{pmatrix} \mathbf{p}_i^T & \mathbf{v}_i^T \end{pmatrix}^T = \begin{pmatrix} x_i & y_i & z_i & v_{x_i} & v_{y_i} & v_{z_i} \end{pmatrix}^T \tag{32}$$

To find velocity vectors that satisfy the no-drift requirement, the system

$$\delta\mathbf{e}_{di} = M(\mathbf{e}_1) \begin{pmatrix} \mathbf{p}_{di} \\ \mathbf{v}_{di} \end{pmatrix} \quad \forall \;\; i = 1 \ldots n \tag{33}$$

must be solved with the additional constraint that the semimajor axis element of $\delta\mathbf{e}_{di}$ be equal to zero for all spacecraft in the formation ($n = 4$ for a tetrahedron formation). In this system, the elements of $\delta\mathbf{e}_{di}$ and $\mathbf{v}_i$ are allowed to vary, while the matrix $M$ and the vectors $\mathbf{x}_i$ are determined by the reference orbit and the tetrahedron geometry, respectively. The system has $9n$ variables and $7n$ constraints and will, therefore, have many possible solutions. In Ref. 13, the velocity magnitude is chosen to achieve the no-drift condition and the ECI velocity direction of each spacecraft in the formation is chosen to match the direction of reference orbit's velocity vector. This method will succeed in creating a drift-free formation, however it does not take into account the states of the spacecraft in the formation immediately prior to initialization.

The approach presented here minimizes the size of the maneuvers that would be required to create the desired formation. The approach selects initial conditions, $\delta\mathbf{e}_{di}$, that are closest to the current differential states, $\delta\mathbf{e}_i$, of the spacecraft in the formation and that will minimize the state error, $\zeta_{0i}$, across the formation at the start of the initialization. For the entire formation, this criterion becomes

$$\min_{\delta\mathbf{e}_{di}, \mathbf{v}_{di} \;\; \forall i=1\ldots n} \sum_{i=1}^{n} \|W_i(\delta\mathbf{e}_{di} - \delta\mathbf{e}_i)\|_1 \tag{34}$$

where $W_i$ are weighting matrices that represent the expected fuel-cost of changing orbital elements (obtainable from the GVEs). Allowing different $W_i$ for each spacecraft enables the formation design to take into account factors such as fuel-weighting to extend overall mission duration, similar to the approach used in choosing the *virtual center* in Ref. 20. The use of a 1-norm is appropriate in this case, because the distance that a given element must be changed is the absolute value of the difference between that element's current and desired state. This approach is similar to the optimization used in Ref. 2, in which drift-free, minimum maneuver constants of integration were found for Lawden's Equations. Next, the optimization is expanded by exploiting specific aspects of the MMS mission science goals.

The *quality* of the shape of the regular tetrahedron[a] largely determines the value of the science data recovered by a mission such as MMS.[14] In choosing the initial conditions for a regular tetrahedron-shaped

[a] Tetrahedron quality is discussed in Ref. 19

formation, certain quantities that do not affect shape quality such as the scale, position, and orientation of the tetrahedron can be considered degrees of freedom in the optimization described by Eqs. 33 and 34. By optimizing the additional degrees of freedom, tetrahedron-shaped initial conditions can be found that require smaller maneuvers to achieve from the current formation state. Scaling the tetrahedron shape equally in three dimensions introduces a single scalar variable $s$ and allowing translation in each orthogonal direction of the LVLH frame introduces the variables $t_x$, $t_y$, and $t_z$. The new constraint set is

$$\delta\mathbf{e}_{di} = M(\mathbf{e}_1)\left[\begin{pmatrix} s\mathbf{p}_{di} \\ \mathbf{v}_{di} \end{pmatrix} + \mathbf{t}\right] \quad , \quad \begin{pmatrix} 1 & 0 & 0 & 0 & 0 & 0 \end{pmatrix}\delta\mathbf{e}_{di} = 0 \qquad \forall \;\; i = 1\ldots n \tag{35}$$

where $\mathbf{t} = \begin{pmatrix} t_x & t_y & t_z & 0 & 0 & 0 \end{pmatrix}^T$ and the second constraint forces a no-drift condition by ensuring that the relative semimajor axes, the first element of each $\delta\mathbf{e}_{di}$ vector, are zero. These constraints can be combined with the objective in Eq. 34 and formulated as a linear program. In addition to the geometric and no-drift constraints, limits on the desired differential angle state variables are required to ensure that they remain within $\pm\pi$ and on eccentricity and semimajor axis to ensure that the spacecraft remain in Earth orbit.

For elliptical orbits, it is not possible to maintain constant relative geometry between satellites for all points in the orbit. Instead, a single position in the orbit must be chosen for the satellites to form a tetrahedron. The mean anomaly at the time of the tetrahedron geometry will be $M_t$. When formulating the optimization in Eqs. 34 and 35, the current differential element vectors $\zeta_{0i}$ must be propagated forward using the state transition matrix in Section A to the mean anomaly $M_t$. In addition, the reference orbit used to compute the matrix $M(\mathbf{e}_1)$ should have a mean anomaly set to $M_t$.

There are several limitations to this optimization approach. First, it does not optimally assign spacecraft to positions in the tetrahedron (a formulation that does this is possible using mixed integer linear programming or network LP[4,16]). Second, the optimization posed here does not optimally orient the tetrahedron in three space. Introducing a rotation matrix dependent on three Euler parameters would create a nonlinear optimization. This limitation could be bypassed by creating a spherical lattice about the orbit and optimizing the formation rotated once for each point on the lattice. After performing all the optimizations, the desired state corresponding to the rotation with the lowest cost would be chosen. Although this approach requires a preset number of optimizations (possibly many depending upon the degree of rotation resolution desired), the optimizations are small linear programs, which complete in a fraction of a second.

An alternative form of Eq. 35 can be written to allow for small rotations using the linearized form of a three-dimensional rotation matrix[12]

$$\mathbf{x}' = \begin{pmatrix} 1 & \theta_z & -\theta_y \\ -\theta_z & 1 & \theta_x \\ \theta_y & -\theta_x & 1 \end{pmatrix}\mathbf{x} \equiv \mathbf{R}\mathbf{x} \tag{36}$$

where $\theta_x$ is the rotation about the $x$ axis, $\theta_y$ is the rotation about the $y$ axis, $\theta_z$ is the rotation about the $z$ axis, $\mathbf{x}$ is an arbitrary LVLH position vector, and $\mathbf{x}'$ is the vector $\mathbf{x}$ after having been rotated. Using Eq. 36 in Eq. 35 yields

$$\delta\mathbf{e}_{di} = M(\mathbf{e}_1)\left[\begin{pmatrix} \mathbf{R} & \mathbf{0}_3 \\ \mathbf{0}_3 & \mathbf{I}_3 \end{pmatrix}\begin{pmatrix} \mathbf{p}_{di} \\ \mathbf{v}_{di} \end{pmatrix} + \mathbf{t}\right] \quad , \quad \begin{pmatrix} 1 & 0 & 0 & 0 & 0 & 0 \end{pmatrix}\delta\mathbf{e}_{di} = 0 \qquad \forall \;\; i = 1\ldots n \tag{37}$$

where $\mathbf{R}$ is the rotation matrix defined in Eq. 36, $\mathbf{0}_3$ is a $3\times 3$ matrix of zeros, and $\mathbf{I}_3$ is a $3\times 3$ identity matrix. The variables being chosen in the new optimization are the vectors $\delta\mathbf{e}_{di}$, the rotations $\theta_x$, $\theta_y$, and $\theta_z$ (contained in $\mathbf{R}$), the velocities $\mathbf{v}_{di}$, and the translations $\mathbf{t}$. The optimization can perform small rotations ($\theta_x$, $\theta_y$, and $\theta_z$ are constrained), but can no longer optimize the tetrahedron scale and still retain linearity. Ref. 20 contains more detailed analysis of this initialization method.

## V. Formation Maintenance on MMS-like Mission

The control system described in Section III was demonstrated on a segment of the MMS mission. The MMS mission is comprised of four spacecraft that create regular tetrahedron geometries once per orbit. The orbits of the four spacecraft are widely separated and highly elliptical, presenting a challenge for many optimal formation specification and control approaches in the literature.[1,2] Using the tetrahedron initial-condition optimization approach in Section IV and the model predictive approach in Section III, the four spacecraft were controlled in a fully nonlinear simulation with Earth oblateness effects, atmospheric drag

effects, and sensing noise (2 cm position, 0.5 mm/s velocity) using a commercial orbit propagator.[21] The control objective in this simulation is to achieve a set of tetrahedron initial conditions once per day near the formation orbit apogee.

In order to implement the MPC scheme in Section III using the dynamics developed in Section II, the second method of calculating $\Gamma$ in subsection II.C is used. The dynamics matrices $\Gamma$, $\bar{\Phi}$, and $D$ are all functions of the desired orbital elements, which are parameter-varying. To obtain accurate trajectories for the desired orbital elements, they are integrated numerically with $J_2$ disturbance effects included and then used to generate the linear propagation matrices used in the optimization. The desired trajectories of each satellite only need to be recalculated when the desired orbits change.

Figure 3(a) shows the rate at which fuel was used over the course of one week of formation flying. The formation fuel use rate converges to approximately 12.1 mm/s per day ($\approx$ 1 orbit) for each satellite. Another simulation performed with dynamics that did not include the effects of $J_2$ indicates 11.5 mm/s are used per satellite for a similar orbit. The state error for one of the spacecraft in the formation is seen being driven to the origin in Figure 3(b). Trajectories followed during this simulation terminated within the range of acceptable state error determined for the linearizing assumptions used in Section II.

## VI. Conclusion

A variant of Gauss' Variational Equations that incorporates the effects of $J_2$ has been used to derive a set of linearized relative dynamics of orbital motion. Using this linear parameter varying dynamics model extends previous work on orbital element planning controllers. By accounting for $J_2$ disturbances in the dynamics the planning controller is able to exploit these dynamics for improved fuel efficiency. The linearization assumptions for the new set of dynamics were shown to be valid for typical spacecraft error box sizes. Efficient means of using these dynamics were also introduced and validated. A method of applying rectilinear error box constraints to a formation specified in differential orbital elements was presented. The $J_2$-modified GVE-based dynamics/MPC controller was used to specify and control a large (1km sides) tetrahedron-shaped formation in an MMS-like orbit for a period of seven days using a commercial propagator with realistic disturbances showing that the controller is both reliable and fuel-efficient relative to previous formation flying controllers.

## Acknowledgments

The authors would like to thank Prof. Terry Alfriend for his ideas and suggestions. This work was funded under Cooperative Agreement NCC5-729 through the NASA GSFC Formation Flying NASA Research Announcement. Any opinions, findings, and conclusions or recommendations expressed in this material are those of the author(s) and do not necessarily reflect the views of the National Aeronautics and Space Administration.

## References

[1]M. Tillerson and J. How, "Formation Flying Control in Eccentric Orbits," *Proceedings of the AIAA Guidance, Navigation, and Control Conference*, Montreal, Canada, Aug. 6-9, 2001, 2001.

[2]G. Inalhan, M. Tillerson, and J. How, "Relative Dynamics & Control of Spacecraft Formations in Eccentric Orbits," AIAA Journal of Guidance, Control, and Dynamics (0731-5090), vol. 25, no. 1, Jan.-Feb. 2002, p. 48-59.

[3]G. Franklin, J. Powell, and M. Workman, "Digital Control of Dynamic Systems," Third Edition,Addison-Wesley, 1998.

[4]M. Tillerson, G. Inalhan, and J. How, "Coordination and Control of Distributed Spacecraft Systems Using Convex Optimization Techniques," Int. Journal of Robust and Nonlinear Control, vol 12, Issue 2-3, Feb.-Mar. 2002, p.207-242.

[5]Ilgen, M.R., "Low Thrust OTV Guidance using Lyapunov Optimal Feedback Control Techniques," AAS/AIAA *Astrodynamics Specialist Conference*, Victoria, B.C., Canada, Aug. 16–19 1993, Paper No. AAS 93-680.

[6]B. Naasz, *Classical Element Feedback Control for Spacecraft Orbital Maneuvers,* S.M. Thesis, Dept. of Aerospace Engineering, Virginia Polytechnic Institute and State University, May 2002.

[7]Mishne, D. "Formation Control of LEO Satellites Subject ot Drag Variations and $J_2$ Perturbations," AAS/AIAA Astrodynamics Specialist Conference, Monterey, California, August 2002.

[8]P. Gurfil, "Control-Theoretic Analysis of Low-Thrust Orbital Transfer Using Orbital Elements," *AIAA Journal of Guidance, Control, and Dynamics*, vol. 26, no. 6, November-December 2003, p. 979-983.

[9]H. Schaub and K. T. Alfriend, "$J_2$ Invariant Relative Orbits for Spacecraft Formations," *Flight Mechanics Symposium*, (Goddard Space Flight Center, Greenbelt, Maryland), January 18-20, 2002, Paper No. 11.

[10]H. Schaub and J.L. Junkins, *Analytical Mechanics of Space Systems,* AIAA Education Series, Reston, VA, 2003.

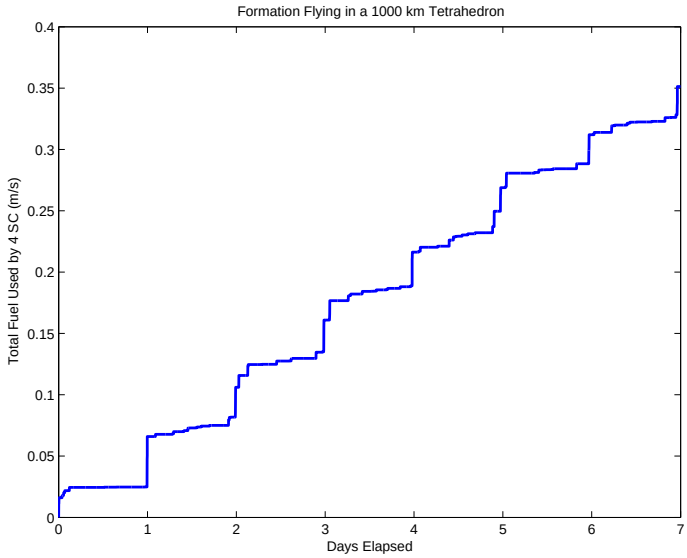


(a) Combined formation fuel use over time

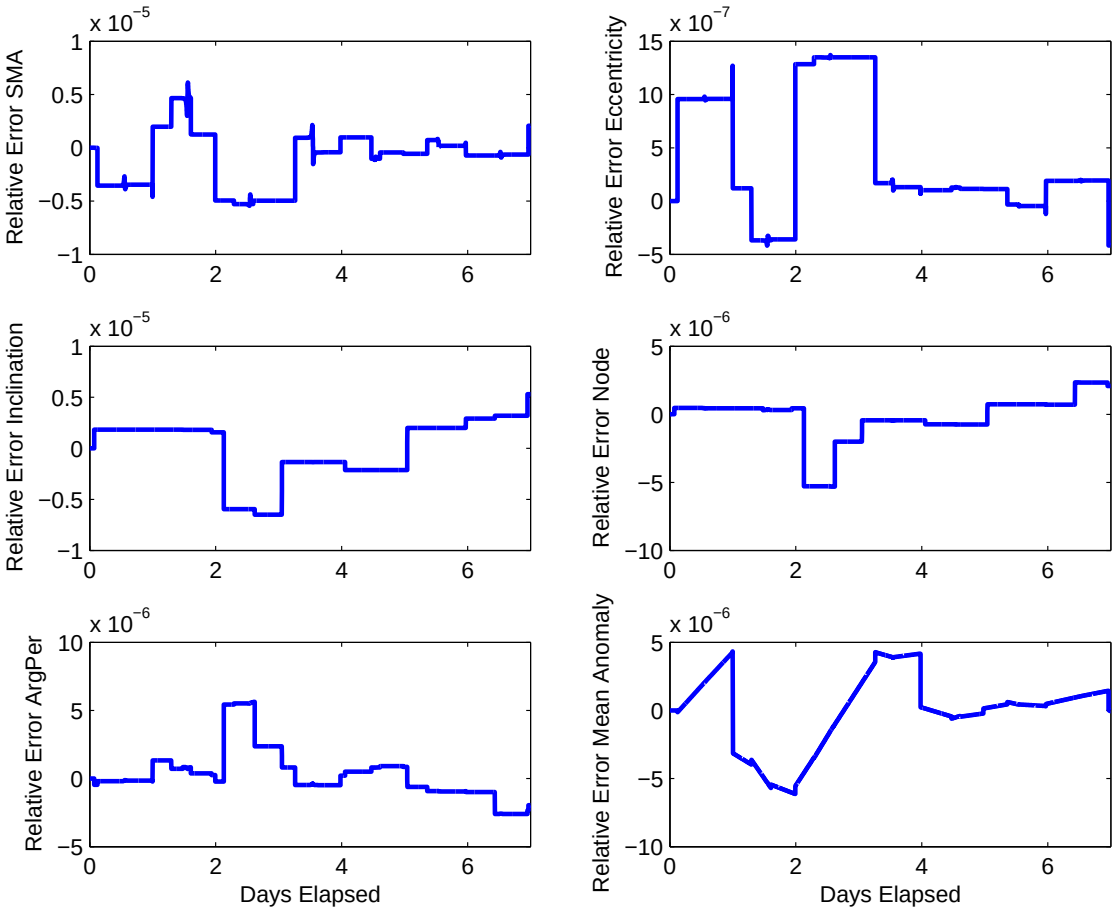


(b) State error for satellite #1

**Fig. 3:** Forming and maintaining a 1000 km tetrahedron formation in a highly eccentric orbit ($e \approx 0.8$) in the presence of $J_2$

[11]Battin, Richard H., *An Introduction to the Mathematics and Methods of Astrodynamics,* AIAA Education Series, New York, 1987.

[12]Greenwood, D.T., *Advanced Dynamics,* Cambridge University Press, Cambridge, 2003.

[13]J. Guzman and C. Schiff, "A Preliminary Study for a Tetrahedron Formation - Quality Factors and Visualization (Spacecraft Formation Flying)," *AIAA/AAS Astro. Specialists Conf.*, Aug 2002.

[14]P. Robert, A. Roux, C. Harvey, M. Dunlop, P. Daly, and K. Glassmeier, "Tetrahedron Geometric Factors," Analysis Methods for Multi-Spacecraft Data, pp. 323348, Noordwijk, The Netherlands: ISSI Report SR-001, ESA Pub. Div., 1998.

[15]J. R. Carpenter and K. T. Alfriend, "Navigation Accuracy Guidelines for Orbital Formation Flying," AIAA Guidance, Navigation, and Control Confrence, Austin, TX, Aug 11-4, 2003.

[16]D. Bertsimas and J.N. Tsitsiklas, *Introduction to Linear Optimization,* Athena Scientific, Belmont, 1997.

[17]W. Ren, and R. Beard, "Virtual Structure Based Spacecraft Formation Control with Formation Feedback," presented at the *AIAA GN&C Conference,* Aug. 2002.

[18]D.W. Gim and K.T. Alfriend, "State Transition Matrix of Relative Motion for the Perturbed Noncircular Reference Orbit," AIAA Journal of Guidance, Control, and Dynamics, vol. 26, no. 6, Nov.-Dec. 2003, p. 956-971.

[19]L.S. Breger, *Model Predictive Control for Formation Flying Spacecraft*, S.M. Thesis, Massachusetts Institute of Technology, Dept. Aeronautics and Astronautics, June 2004.

[20]J. P. How, T. Alfriend, L. Breger, and M. Mitchell, "Semimajor Axis Estimation Strategies," presented at the *2nd International Formation Flying Symposium ,* Sept. 2004.

[21]A.I. Solutions, "FreeFlyer User's Guide", Version 4.0, March 1999.